




ORIGINAL RESEARCH ARTICLE

Effect of Al₂O₃ Addition on Magnetolectric Properties of Ni_{0.5}Zn_{0.5}Fe₂O₄/Ba_{0.8}Sr_{0.2}TiO₃ Composite Ceramics

XIAOFENG QIN,^{1,2} CHUANG ZHOU,^{1,2} HENG WU,^{1,2} LI CHENG,^{1,2}
TAO FAN,^{1,2} RONGLI GAO ^{1,2,3} ZHIXIN ZENG,^{1,2} and HONGDI WU^{1,2}

1.—School of Metallurgy and Materials Engineering, Chongqing University of Science and Technology, Chongqing 401331, China. 2.—Chongqing Key Laboratory of Nano/Micro Composite Materials and Devices, Chongqing 401331, China. 3.—e-mail: gaorongli2008@163.com

Magnetolectric composites have attracted widespread attention during the past few decades due to their strong magnetolectric coupling effect and potential applications above room temperature. Ni_{0.5}Zn_{0.5}Fe₂O₄/Ba_{0.8}Sr_{0.2}TiO₃ composites have been prepared by the conventional high-temperature solid-state method and the effects of Al₂O₃ addition on their microstructure, dielectric, ferroelectric, and magnetic properties studied. x-Ray diffraction (XRD) analysis confirmed the biphasic structure of the composites. scanning electron microscopy (SEM) showed that addition of a certain amount of Al₂O₃ can enhance the density and promote uniform growth of particle size. The sample with 1 wt.% Al₂O₃ addition exhibited the largest dielectric constant and lowest dielectric loss (< 0.05 at 1 kHz) at high temperature (> 354°C). The sample with 3 wt.% Al₂O₃ addition presented the best ferroelectric properties, with the highest values of residual polarization ($P_r = 2.2150 \mu\text{C}/\text{cm}^2$) and coercive field ($E_c = 30.6527 \text{ kV}/\text{cm}$) among the specimens. The remanent magnetization (M_r) and saturated magnetization (M_s) decreased with increasing Al₂O₃ content. In short, addition of Al₂O₃ caused changes in the grain size, density, and defects, and addition of a certain amount of Al₂O₃ can improve the magnetolectric properties.

Key words: Ceramics, Al₂O₃, structural, magnetolectric performance

INTRODUCTION

The development of new, multifunctional materials has attracted great interest recently with the rapid progress of science and technology.^{1–3} Multiferroic materials in particular have drawn much attention because of their coupling effect and wide range of functions.⁴ By utilizing this magnetolectric coupling property of multiferroic materials, various novel devices such as spintronic devices, transducers, storage devices, and capacitors can be fabricated.⁵ Multiferroic materials with a strong magnetolectric coupling effect form the foundation for preparation of the above-mentioned novel

devices. Multiferroic materials can be divided into single-phase and composite categories. At present, the common single-phase multiferroic materials mainly include bismuth perovskites (BiFeO₃) and manganite perovskites (ReMn_xO_y).^{6,7} However, the Néel temperature (T_N) and Curie temperature (T_C) of most single-phase multiferroic materials are lower than room temperature. To date, the magnetolectric coupling coefficient of single-phase multiferroic materials has remained very small, not meeting application requirements.^{8–12} Xue¹³ reported that ferroelectrics and ferromagnets can be combined to produce multiferroic composites that exhibit a magnetolectric coupling effect. It is generally acknowledged that the magnetolectric coupling effect in composite multiferroic materials occurs due to the magnetostrictive and piezoelectric effects. When such materials are subjected to an

external electric field, the ferroelectric phase generates stress because of the inverse piezoelectric effect.¹⁴ The inverse magnetostrictive effect then occurs in the ferromagnetic phase through stress transfer at the interface, thus changing the magnetization of the material. Similarly, the ferroelectricity of materials can be changed by varying the magnetic field.^{15,16} Besides, the ferroelectric and ferromagnetic phases can also work alone. Compared with single-phase multiferroic materials, composite multiferroic materials have a wide range of fabrication methods and types as well as strong magnetoelectric effects at room temperature, making them more convenient than single-phase multiferroic materials.

To obtain a larger magnetoelectric coupling coefficient, many researchers have carried out extensive experiments by regulating the composition, optimizing the process, varying the testing conditions, etc. However, due to the different sintering temperatures of the constituent phases, it is easy to cause various problems such as cofiring mismatch¹⁷ for different compositions, insufficient bonding of ceramic grains, and hindered stress-strain transfer,¹⁸ which is not conducive to the performance of the sample.¹⁹ To solve these problems, some researchers have optimized the properties of composites by adjusting the composition,²⁰ changing the preparation process,²¹ designing different structures,²² adding combustion aids,²³ etc. On the basis of previous studies, it is known that adding combustion aids can address the mismatch phenomenon during ceramic cofiring, reduce the sintering temperature, and increase the density.^{24–26} Although it is possible to adjust the properties of composite ceramics by adding sintering aids, the grain size, density, etc. will then also change.²⁷ How these factors affect the performance of composite ceramics thus requires further study.

In recent years, various multiferroic composites have been successfully prepared. Ba_{0.8}Sr_{0.2}TiO₃ (BST) is a typical ferroelectric material with dielectric permittivity and resistivity values that are higher than those of many other ferroelectric materials,^{28,29} so it was chosen as the ferroelectric phase in this work. Ni_{0.5}Zn_{0.5}FeO₄ (NZFO) is a conventional magnetic material with high resistivity, strong magnetic permeability, and large magnetic coercivity that is widely used in memories, permanent magnets, etc. and was thus chosen as the magnetic phase.^{30,31} Addition of Al₂O₃ can reduce the sintering temperature of ceramic, and alleviate the ceramic cofiring mismatch issue. Addition of a small amount of Al₂O₃ can result in the formation of a solid solution, thus facilitating sintering to a density close to theoretical, limiting crystal growth, and forming a microstructure with isometric crystals,²⁴ so it was chosen as the sintering aid.³² In the work presented herein, NZFO/BST ceramics were prepared by the solid-phase method and their microstructure and magnetoelectric properties were

studied for different Al₂O₃ contents. Addition of different amounts of Al₂O₃ resulted in changes in the microstructure, ferroelectric and dielectric properties, etc.; For example, if the Al₂O₃ content is too high, the glass phase near the grain boundary may be excessive, which is detrimental to the magnetoelectric properties. It is therefore of great significance to discuss the influence of adding different amounts of Al₂O₃ on the magnetoelectric properties of NZFO/BST composite ceramics to facilitate their use in memories, sensors, microwave devices,⁵ and other fields as well as to provide ideas for optimizing the performance of other types of composite materials.

EXPERIMENTAL PROCEDURES

NZFO/BST ceramics were prepared by a solid-phase method. The starting materials Ni₂O₃ (99%), ZnO (99%), and Fe₂O₃ (99%) were weighed and then mixed and calcined at 900°C in air for 2 h to prepare Ni_{0.5}Zn_{0.5}Fe₂O₄ (NZFO). Simultaneously, a mixture of BaCO₃ (99.8%), SrCO₃ (99%), and TiO₂ (99%) was ball milled and calcined at 1000°C in air for 3 h to synthesize Ba_{0.8}Sr_{0.2}TiO₃ (BST).³³ The NZFO and BST powders were mixed at molar ratio of 1:4. An appropriate amount of NZFO/BST powder was taken and 1 wt.%, 3 wt.%, or 5 wt.% Al₂O₃ was added to obtain the NZFO/BST powder samples. Polyvinyl alcohol (15 wt.%) was added to the NZFO/BST powders, which were then pressed into sheets that were sintered in air for 3 h at 1050°C using a rate of 5°C/min.

The surface morphology of the ceramics was studied by SEM (S-3700N, Hitachi). XRD patterns were collected using an x-ray diffractometer (Rigaku D/max 2400, 40 kV, 30 mA, Cu K_α, λ = 0.15406 nm). The dielectric properties of the NZFO/BST ceramics were characterized by using an LCR digital bridge (E4980A, Agilent). The ferroelectric properties of the ceramics were obtained by using a ferroelectric analyzer (TF2000E, Aix-ACCT) in LM and PM mode, respectively. The hysteresis loops of the ceramics were measured using a vibrating-sample magnetometer (Quantum Design).

RESULTS AND DISCUSSION

Crystal Structure

The XRD patterns of the composites measured at room temperature are shown in Fig. 1. These results show that all the main diffraction peaks could be indexed to (220), (311), (222), (440), (620), (220), and (533) reflections of Ni_{0.5}Zn_{0.5}Fe₂O₄ phase with cubic spinel structure. The perovskite structure of Ba_{0.8}Sr_{0.2}TiO₃ phase was indicated by other diffraction peaks corresponding to (100), (110), (111), (020), (120), (211), and (202).³⁴ No obvious impurity phases were detected. These results confirm the presence of the ferroelectric phase (BST) and ferromagnetic phase (NZFO) in the composite ceramics,

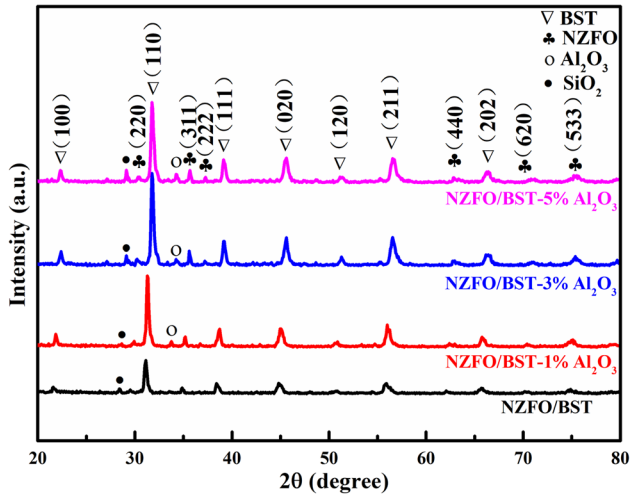


Fig. 1. XRD patterns of NZFO/BST ceramics.

each retaining its respective characteristics.³³ It can be seen from the XRD patterns that, as the Al_2O_3 content was increased, the crystallinity of the ceramic grains first increased then decreased. Among the samples, NZFO/BST-3% Al_2O_3 showed the highest crystallinity, demonstrating that addition of Al_2O_3 was beneficial to grain growth. Also, with increasing Al_2O_3 content, all the diffraction peaks moved to high angle. This may be because addition of Al_2O_3 causes the grains in the ceramic to be squeezed, so that they bond more closely, thereby decreasing the distance between the crystal planes and moving the diffraction peaks to high angle.

Surface Morphology

Figure 2 shows SEM images of the prepared composites, revealing a difference in the surface topography of each sample.³⁵ As seen from Fig. 2, the crystal grains exhibited nonuniform growth and many pores were present on the surface of all the samples; the sample with the least pores on the surface had an Al_2O_3 content of 3%. The average grain size of the specimens was calculated by using Nano Measurer software, and the results are presented in Table I, from which the following conclusions can be drawn. Firstly, with increasing Al_2O_3 content, the grain size first increased then decreased, and the average grain size was largest when the Al_2O_3 content was 1% (207.47 nm). With increasing Al_2O_3 content, the density first increased then decreased, reaching its largest value (6.04 g/cm³) when the Al_2O_3 content was 3%. From these results it can be inferred that addition of Al_2O_3 can not only increase the density but also promote the growth of crystal grains to a certain extent.

Dielectric Properties

Temperature has a great influence on the dielectric constant (ϵ_r), so we studied the dielectric properties of the composites using the relationship between the dielectric constant and temperature. The ϵ_r of the composites with different Al_2O_3 contents is shown as a function of temperature in Fig. 3. Two relaxation peaks are observed at low frequencies (1 kHz), at about 50°C and 450°C. The peak intensity was highest when 1% Al_2O_3 was added. As the temperature was increased, the value of ϵ_r first decreased then increased; moreover, it decreased with increasing frequency. As the temperature was increased, a larger number of electrons are transferred from the valence to conduction band, which is equivalent to an enhancement in polarization.³⁶ Therefore, in practice, the dipoles $\text{Fe}^{3+} \Leftrightarrow \text{Fe}^{2+}$ are oriented with their axes parallel to the applied field, thereby contributing to an increase in the ϵ_r value, while there also is an inherent ionic polarization in the ferrite that is also beneficial to polarization.³⁷ When the frequency is lower and the temperature is higher, these mechanisms are more effective. However, when the temperature rises to a certain extent, the ionic thermal motion energy becomes very large and the directional migration of ions under the action of the electric field is hindered by thermal motion, thus weakening the polarization. At this point, the loss increases significantly (Fig. 4).

Figure 4 shows the dielectric loss ($\tan \delta$) of the composites as a function of temperature at different frequencies. Overall, the $\tan \delta$ value increases with increasing temperature but decreases with increasing frequency.³⁵ As the temperature is increased, many electrons will be promoted from the valence to conduction band, which can increase the conductivity of the NZFO phase, leading to an increase in the conductivity loss of the ceramic.³⁶ The peaks will shift to high-temperature regions as the frequency increases because of the thermally activated relaxation mechanism.^{38,39} According to the Arrhenius law,⁴⁰ the relaxation time is plotted versus temperature in Fig. 5 inset.

$$\tau = \tau_0 \exp(E_a / (k_B T)), \quad (1)$$

where τ_0 is the preexponential factor, E_a is the activation energy, and k_B is the Boltzmann constant. The E_a value of all the samples was obtained by linear fitting (as illustrated in Fig. 4), yielding values of 1.34 eV, 1.62 eV, 1.16 eV, and 1.40 eV for E_a values for the NZFO/BST, NZFO/BST-1% Al_2O_3 , NZFO/BST-3% Al_2O_3 , and NZFO/BST-5% Al_2O_3 sample, respectively. Oxygen vacancies can affect the dielectric properties and thereby the activation energy.^{38,41}

In addition to the temperature, the frequency is another important factor affecting the dielectric properties of the samples. Figure 5 shows the dielectric loss ($\tan \delta$) and dielectric constant (ϵ_r) of

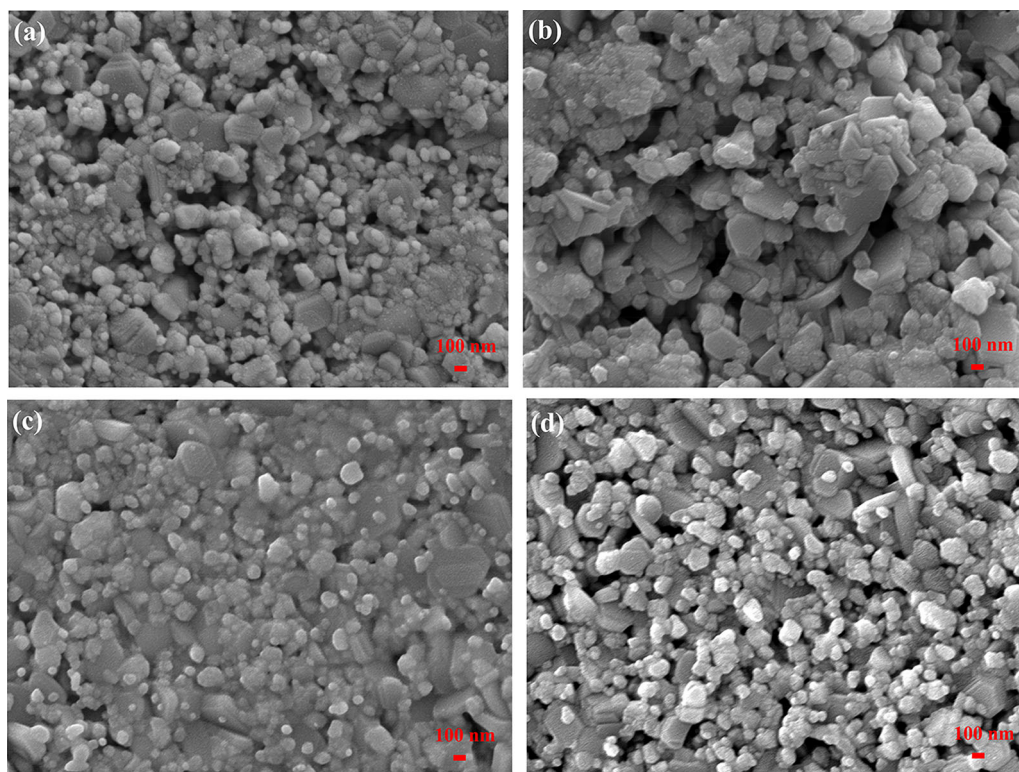


Fig. 2. SEM images of composite ceramics: (a) NZFO/BST, (b) NZFO/BST-1%Al₂O₃, (c) NZFO/BST-3%Al₂O₃, and (d) NZFO/BST-5%Al₂O₃.

Table I. Average grain size and density of ceramics with different Al₂O₃ contents

Al ₂ O ₃ (wt.%)	0	1	3	5
Average grain size (nm)	171.31	207.47	198.88	193.00
Density (g/cm ³)	4.78	5.44	6.04	5.15

the ceramics with different Al₂O₃ contents as functions of frequency at room temperature. The values of $\tan \delta$ and ϵ_r decline rapidly in the low frequency region ($f < 10^4$ Hz), while they decline slightly when the frequency exceeds 10^4 Hz. This is mainly caused by relaxation polarization. Since the polarization time of dipole rotation polarization and space charge polarization is rather long, they cannot be established at high frequencies,^{42,43} thus the relaxation polarization decreases with increasing frequency and ϵ_r decreases with increasing frequency. Moreover, ϵ_r declines as the content of Al₂O₃ is increased, so the NZFO/BST-3%Al₂O₃ and NZFO/BST-5%Al₂O₃ samples show great frequency

stability. Al₂O₃ is a nonelectrolyte, so although its addition will enhance the density, it acts like an impurity in the composite ceramics, meaning that its addition may result in a decrease of the ϵ_r value.

The frequency dependence of the dielectric loss ($\tan \delta$) is similar to that of the dielectric constant; i.e., it decreases monotonically as the frequency is increased. The relaxation loss contributes to the dielectric loss in the low frequency ($f < 10,000$ Hz) region but follows the Maxwell–Wagner law when the frequency increases further.^{42,44} Also, $\tan \delta$ decreases with increasing Al₂O₃ content over most of the frequency range ($f > 200$ Hz). This finding can be deduced from Fig. 2. Because Al₂O₃ can form a liquid phase at grain boundaries, the number of pores in the sample is reduced and the leakage conduction loss is reduced.

Ferroelectric Properties

Figure 6 shows the hysteresis loop (P – E curve) of the NZFO/BST composite ceramics with different Al₂O₃ contents measured at room temperature at a frequency of 2 kHz. Table II presents the values of the residual polarization (P_r), maximum polarization (P_{max}), and coercive field strength (E_c) of the samples. It can be seen that, with increasing Al₂O₃

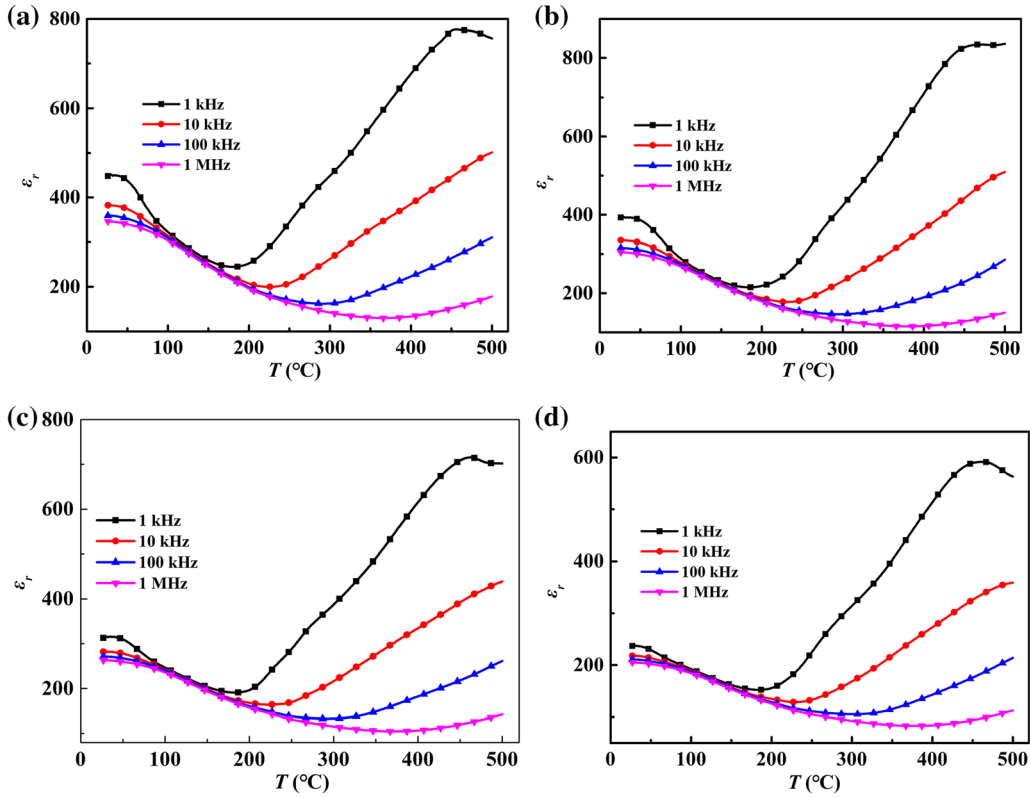


Fig. 3. Dielectric constant (ϵ_r) of the composite ceramics as a function of temperature: (a) NZFO/BST, (b) NZFO/BST-1% Al_2O_3 , (c) NZFO/BST-3% Al_2O_3 , and (d) NZFO/BST-5% Al_2O_3 .

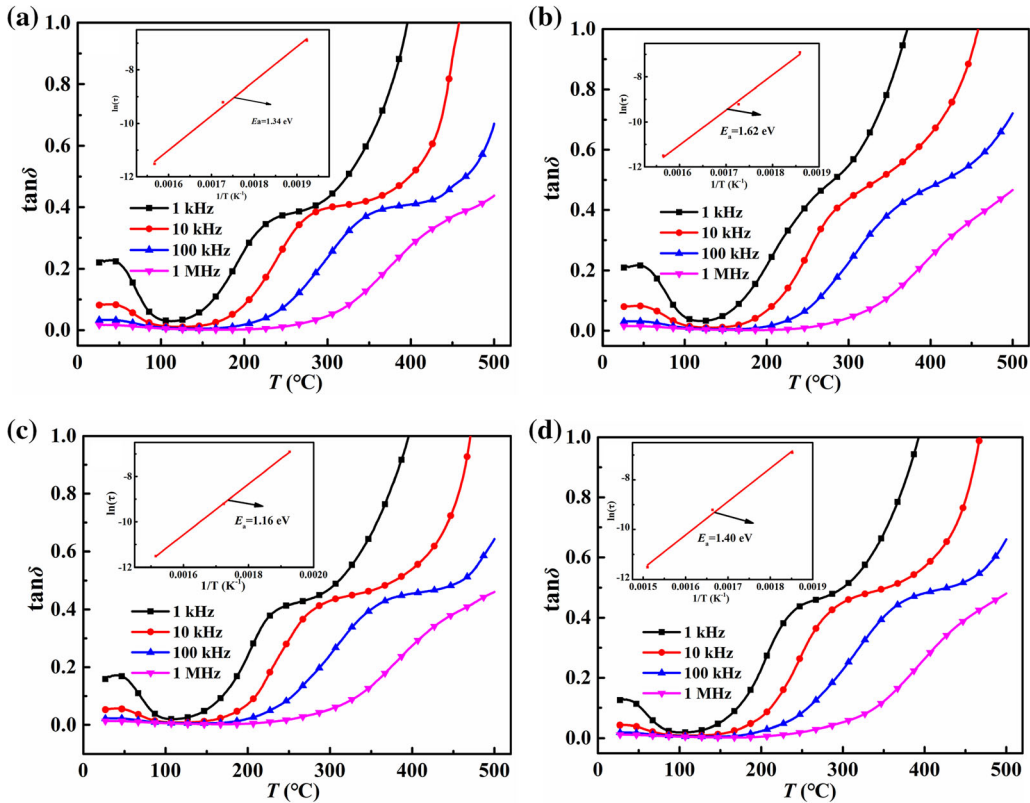


Fig. 4. Dielectric loss ($\tan \delta$) of composites as a function of temperature: (a) NZFO/BST, (b) NZFO/BST-1% Al_2O_3 , (c) NZFO/BST-3% Al_2O_3 , and (d) NZFO/BST-5% Al_2O_3 .

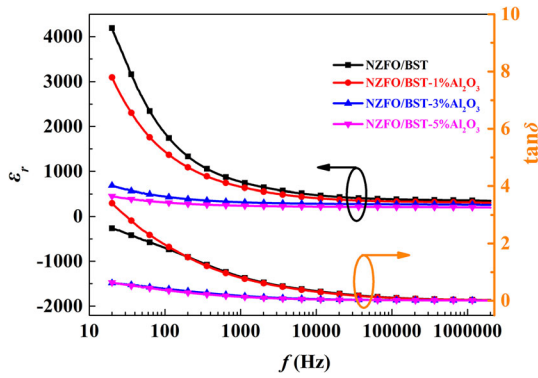


Fig. 5. Dielectric loss ($\tan \delta$) and dielectric constant (ϵ_r) of composites as function of frequency.

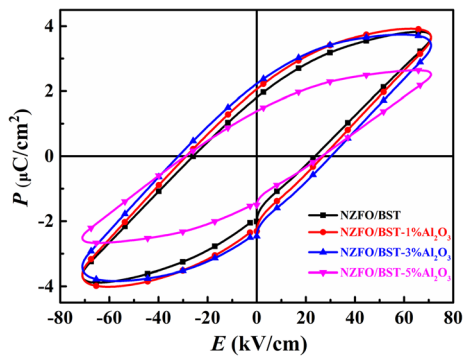


Fig. 6. Hysteresis loops of NZFO/BST ceramics with different Al₂O₃ contents.

Table II. Ferroelectric parameters of NZFO/BST composites with different Al₂O₃ contents.

Al ₂ O ₃ (wt.%)	0	1	3	5
P_{\max} ($\mu\text{C}/\text{cm}^2$)	3.8054	3.9172	3.7724	2.6276
P_r ($\mu\text{C}/\text{cm}^2$)	1.7915	2.0461	2.2150	1.3757
E_c (kV/cm)	23.4233	27.5150	30.6572	26.8181

content, P_r first increases then decreases. Figure 6 clearly shows that the ferroelectric properties of the NZFO/BST-1%Al₂O₃ and NZFO/BST-3%Al₂O₃ samples were better than those of the NZFO/BST sample; in contrast, the xNZFO/BST-5%Al₂O₃ sample exhibited the worst ferroelectric performance. According to the liquid-phase sintering principle,^{45,46} Al₂O₃ is favorable for crystallizing grains during the sintering process. As the Al₂O₃ content is increased, the grains gradually grow, resulting in a higher P_r value for the NZFO/BST-3%Al₂O₃ than NZFO/BST-1%Al₂O₃ sample. As the Al₂O₃ content is further increased, due to excessive doping, the ferroelectric properties weaken, thus the P_r value of the NZFO/BST-5% Al₂O₃ sample is lower.

The leakage current contributes to the measured value of the polarization.³⁵ To minimize its influence, the P - E curves were measured at different frequencies and room temperature (Fig. 7). These results prove that, as the frequency is increased, the curves for all samples become thinner, P_r decreases, while E_c first decreases then increases. It can be inferred that the value of the polarization measured at high frequencies is closer to the intrinsic value for the sample. Although P_r reaches its smallest value at 3 kHz, the squareness of the curve is better at 2 kHz than 3 kHz, and the E_c value is smallest at 2 kHz. Based on these findings, as shown in Fig. 6, the effect of addition of different amounts of Al₂O₃ on the hysteresis loop at 2 kHz was investigated.

On the basis of the discussion above, the leakage current is an important factor that affects the measured value of the polarization. To explore its effect, the J - E curves of the composites with different Al₂O₃ contents were measured (Fig. 8). Under the action of an electric field, addition of Al₂O₃ will increase the leakage current density of the composite ceramics, because Al₂O₃ forms a liquid phase at grain boundaries between the ferroelectric and ferromagnetic phases during the sintering process, causing some carriers to concentrate at the grain boundaries.⁴⁷ Under the action of an external electric field, these carriers will move directionally, resulting in an increase in the leakage current. When the Al₂O₃ content was 3%, the leakage current was the largest. Many factors can affect the leakage current, such as the grain size, grain shape, impurities, density, and other defects.⁴⁸ It is obvious that the variation trend of the average grain size, density, and leakage current was different (Table I). Therefore, the grain size and density are not the most important reason causing the leakage current. When electrons are exchanged between Fe³⁺ and Fe²⁺, oxygen vacancies and other defects may be formed in ceramic samples,⁴⁹ so such defects may be the cause of the high leakage currents observed.

Magnetic Properties

Figure 9 shows the M - H curves of the ceramics with different Al₂O₃ contents, while the corresponding data are presented in Table III. The magnetic properties of the composite ceramics varied with their Al₂O₃ content. The magnetic moment per unit area and grain size are the main factors affecting the magnetic properties. Since Al₂O₃ is a nonmagnetic material, its addition can reduce the magnetic moment per unit area, thus decreasing the saturation magnetization (M_s).

CONCLUSIONS

NZFO/BST composite ceramics with Al₂O₃ added as a combustion aid were successfully synthesized by the conventional high-temperature solid-state method. XRD analysis revealed that no apparent

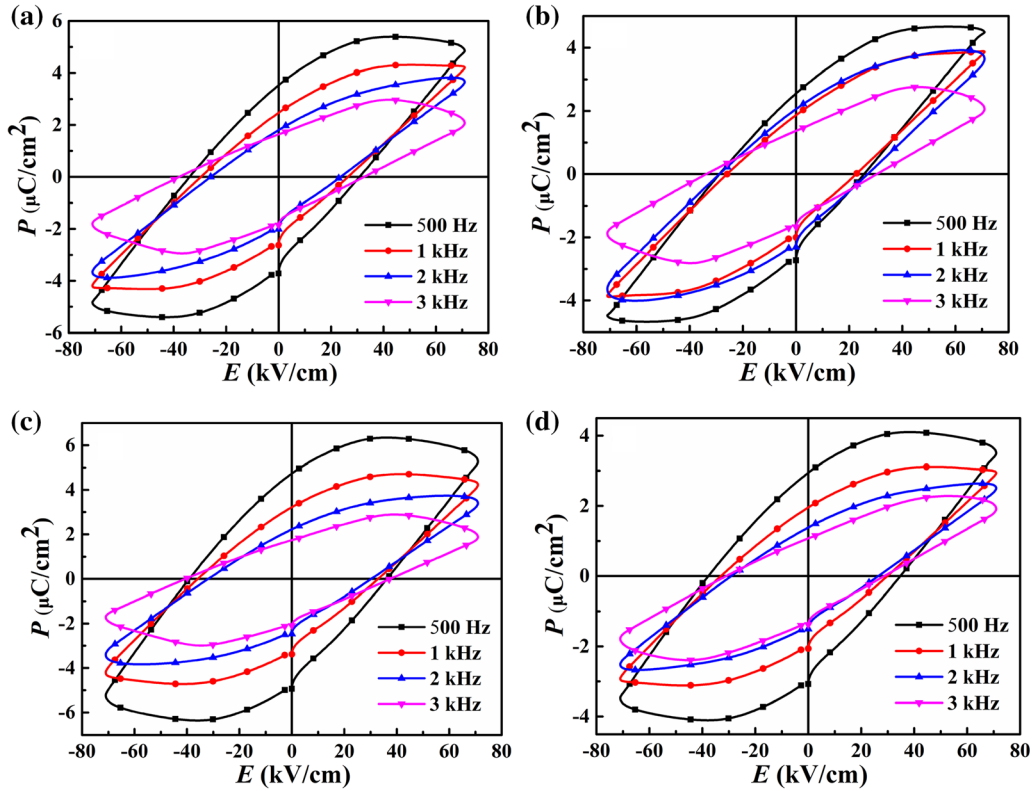


Fig. 7. P - E curves of ZFO/BST composites with different Al_2O_3 contents: (a) NZFO/BST, (b) NZFO/BST-1% Al_2O_3 , (c) NZFO/BST-3% Al_2O_3 , and (d) NZFO/BST-5% Al_2O_3 .

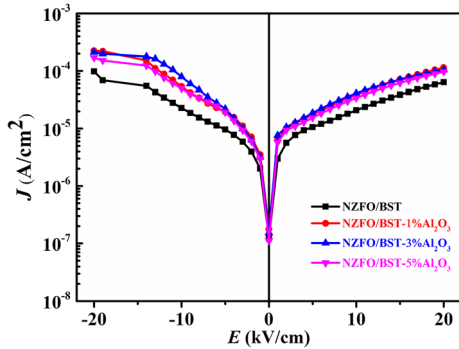


Fig. 8. Leakage current versus applied field for the composite ceramics.

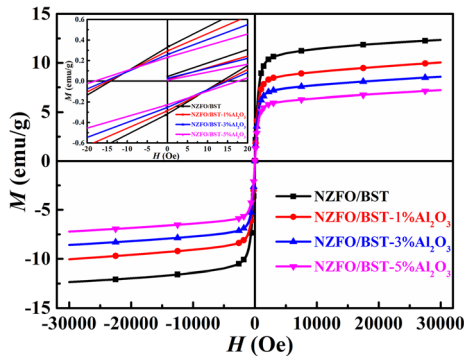


Fig. 9. Magnetization versus magnetic field for the composite ceramics.

Table III. Magnetic parameters of NZFO/BST ceramics with different Al_2O_3 contents

Al_2O_3 (wt.%)	0	1	3	5
M_{\max} (emu/g)	10.9298	8.3764	7.1039	6.1011
M_r (emu/g)	0.3341	0.2909	0.2550	0.2264

second phases formed during the sintering process and that addition of Al_2O_3 was beneficial to increase the degree of crystallinity of the grains. The average grain size ranged from 170 nm to 210 nm with increasing Al_2O_3 content. Al_2O_3 is not only conducive to growth of crystal grains but also plays an active role in enhancing the density. As the Al_2O_3 content was increased, ϵ_r and $\tan \delta$ tended to decrease. Many factors including the testing frequency, testing temperature, number of pores, and density can apparently affect the dielectric properties of the material. All the P - E curves became slimmer at high frequencies, indicating that the leakage current has an important influence on the polarization. When the amount of Al_2O_3 added was 3%, the leakage current was the largest, but the ferroelectricity was also the best, with P_r and E_c values of 2.2150 $\mu\text{C}/\text{cm}^2$ and 30.6572 kV/cm, respectively. The M_s value decreased as the Al_2O_3 content

was increased, mainly being affected by the magnetic moment per unit volume.

ACKNOWLEDGMENTS

The present work has been supported by the Scientific and Technological Research Program of Chongqing Municipal Education Commission (KJZD-M201901501 and KJQN201801509), Chongqing Research Program of Basic Research and Frontier Technology (CSTC2018jcyjAX0416 and CSTC2019jcyj-msxmX0071), Program for Creative Research Groups in University of Chongqing (CXQT19031), Innovation Program for Chongqing's Overseas Returnees (cx2019159), Natural Science Foundation of Chongqing (cstc2020jcyj-zdxmX0008 and cstc2020jcyj-msxmX0030), Leading Talents of Scientific and Technological Innovation in Chongqing (CSTCCXLJRC201919), special project of Chongqing technology innovation and application development (cstc2020jscx-msxmX0218), Science and Technology Research Program of Chongqing Municipal Education Commission (KJZD-M201901501), Excellent Talent Project in University of Chongqing (Grant No. 2017-35), Science and Technology Innovation Project of Social Undertakings and Peoples Livelihood Guarantee of Chongqing (cstc2017shmsA90015), Program for Innovation Teams in University of Chongqing, China (CXTDX201601032), Program for Technical and Scientific Innovation Led by Academician of Chongqing, Latter Foundation Project of Chongqing University of Science and Technology (CKHQZZ2008002), Scientific and Technological Achievements Foundation Project of Chongqing University of Science and Technology (CKKJCG2016328), Postgraduate technology innovation project of Chongqing University of Science & Technology (YKJJCX1820214), and student innovating projects of science of Chongqing (YKJJCX1820205).

CONFLICT OF INTEREST

The authors declare that they have no conflicts of interest.

REFERENCES

- R.L. Gao, Q.M. Zhang, Z.Y. Xu, Z.H. Wang, G. Chen, X.L. Deng, C.L. Fu, and W. Cai, *Compos. B*, 2019, 166, p 204–212.
- S.S. Zhao, Z.Y. Zhou, B. Peng, M.M. Zhu, M.M. Feng, Q. Yang, Y. Yan, W. Ren, Z.G. Ye, Y.H. Liu, and M. Liu, *Adv. Mater.*, 2017, 29, p 1606478.
- R.L. Gao, H.W. Yang, Y.S. Chen, J.R. Sun, Y.G. Zhao, and B.G. Shen, *Appl. Phys. Lett.*, 2014, 104, p 031906.
- H.B. Yang, H. Wang, F. Xiang, and X. Yao, *J. Am. Ceram. Soc.*, 2009, 92, p 2005.
- R.L. Gao, Q.M. Zhang, Z.Y. Xu, Z.H. Wang, W. Cai, G. Chen, X.L. Deng, X.L. Cao, X.D. Luo, and C.L. Fu, *Nanoscale*, 2018, 10(26), p 11750–11759.
- J. Ma, J.M. Hu, Z. Li, and C.-W. Nans, *Adv. Mater.*, 2011, 42, p 1062.
- R.L. Gao, L. Bai, Z.Y. Xu, Q.M. Zhang, Z.H. Wang, W. Cai, G. Chen, X.L. Deng, and C.L. Fu, *Adv. Electron. Mater.*, 2018, 4(6), p 1800030.
- J. Wang, J.B. Neaton, H. Zheng, V. Nagarajan, S.B. Ogale, B. Liu, D. Viehland, and V. Vaithya, *Science*, 2003, 299, p 1719.
- R.L. Gao, Y.Z. Xue, Z.H. Wang, G. Chen, C.L. Fu, X.L. Deng, X. Lei, and W. Cai, *J. Mater. Sci. Mater. Electron.*, 2020, 31(9026), p 9036.
- N. Ikeda, H. Ohsumi, K. Ohwada, K. Ishii, T. Inami, K. Kakurai, Y. Murakami, K. Yoshii, S. Mori, Y. Horibe, and H. Kitô, *Nature*, 2005, 436, p 1136.
- R.L. Gao, Z.H. Wang, G. Chen, X.L. Deng, W. Cai, and C.L. Fu, *Ceram. Int.*, 2018, 44, p S84–S87.
- F. Manfred, *J. Phys. D Appl. Phys.*, 2005, 8, p R123.
- Y.Z. Xue, R.C. Xu, Z.H. Wang, R.L. Gao, C.Y. Li, G. Chen, X.L. Deng, W. Cai, and C.L. Fu, *J. Electron. Mater.*, 2019, 48(8), p 4806–4817.
- Y. Huan, X.H. Wang, J. Fang, and L.T. Li, *J. Eur. Ceram. Soc.*, 2014, 34, p 1445.
- R.C. Xu, S.L. Zhang, F.Q. Wang, Q.W. Zhang, Z.D. Li, Z.H. Wang, R.L. Gao, and C.L. Fu, *J. Electron. Mater.*, 2019, 48, p 386–400.
- M.I. Bichurin, and V.M. Petrov, *J. Low Temp. Phys.*, 2010, 36, p 544.
- R. Zuo, L. Li, and Z. Gui, *J. Mater. Sci. Mater. El.*, 2001, 12, p 117.
- Z. Cheng, H. Zhou, and L. Lin, *Acta Mater.*, 2014, 72, p 239.
- C.Y. Li, R.C. Xu, R.L. Gao, Z.H. Wang, G. Chen, X.L.G. Deng, W. Cai, C.L. Fu, and Q.T. Li, *Mater. Chem. Phys.*, 2020, 249, p 123144.
- D.D. Mishra, D.M. Tewelde, and M. Wang, *J. Mater. Sci.*, 2019, 11, p 10830.
- X.F. Qin, R.C. Xu, H. Wu, R.L. Gao, Z.H. Wang, G. Chen, C.L. Fu, X.L. Deng, and W. Cai, *Process. Appl. Ceram.*, 2019, 13, p 349–359.
- B. Zhao, H.L. Liu, J. Wang, C.Z. Huang, H.T. Zhu, and X.F. Liu, *Ceram. Int.*, 2019, 5, p 49.
- X. Jin, H.C. Zhao, and Y.Q. Li, *Safety & EMC*, 2018.
- R. Gao, X. Qin, Q. Zhang, Z. Xu, Z. Wang, C. Fu, G. Chen, X. Deng, and W. Cai, *J. Alloys Compd.*, 2019, 795, p 501.
- M.L. Pantoya, and J.J. Granier, *Propell. Explos. Pyrotech.*, 2005, 1, p 53.
- R.L. Gao, Q.M. Zhang, Z.Y. Xu, Z.H. Wang, G. Chen, C.L. Fu, X.L. Deng, and W. Cai, *ACS Appl. Electron. Mater.*, 2019, 7, p 1120.
- S. Bajpai, and P.K. Bajpai, *J. Mater. Sci.*, 2019, 10, p 6306.
- R.L. Gao, X.F. Qin, H.L. Duan, H. Wu, R.C. Xu, Q.W. Zhang, S.L. Zhang, and Z.D. Li, *J. Mater. Sci. Mater. El.*, 2020, 31, p 13730–13745.
- J. Paletto, G. Grange, R. Goutte, and L. Eyraud, *J. Phys. D Appl. Phys.*, 1974, 7, p 78.
- R.L. Gao, X.F. Qin, T. Fan, R.C. Xu, H. Wu, Z.H. Wang, G. Chen, C.L. Fu, X.L. Deng, and W. Cai, *J. Mater. Sci. Mater. El.*, 2020, 3, p 2436.
- B. Xiao, Y. Tang, P.Y. Du, and H. Wang, *Ceram. Int.*, 2020, <https://doi.org/10.1016/j.ceramint.2020.08.025>.
- A.K. Moe, E.S. Lukin, and N.A. Popova, *Refract. Ind. Ceram.*, 2018, 4, p 342.
- C. Zhou, W. Cai, Q.W.Z.H.D. Wu, H. Wu, R.L. Gao, G. Chen, Z.H. Wang, X.L. Deng, and C.L. Fu, *Mater. Chem. Phys.*, 2020, 258, p 124001.
- C. Zhu, H. Tu, Y. Bai, D. Ma, and Y.G. Zhao, *Fuel*, 2019, 254, p 15730.
- R.L. Gao, X.F. Qin, Q.M. Zhang, Z.Y. Xu, Z.H. Wang, C.L. Fu, G. Chen, X.L. Deng, and W. Cai, *Mater. Chem. Phys.*, 2019, 232, p 428.
- S.B. Li, C.B. Wang, Q. Shen, M.Z. Hu, and L.M. Zhang, *J. Alloys Compd.*, 2018, 762, p 415.
- X.F. Qin, H. Wu, R.C. Xu, R.L. Gao, Z.H. Wang, G. Chen, C.L. Fu, X.L. Deng, and W. Cai, *J. Mater. Sci. Mater. El.*, 2020, 31, p 4073–4082.
- R. Sharma, P. Pahuja, and R.P. Tandon, *Ceram. Int.*, 2014, 40, p 9027.

39. Q.T. Li, Q.W. Zhang, W. Cai, C. Zhou, R.L. Gao, G. Chen, X.L. Deng, Z.H. Wang, and C.L. Fu, *Mater. Chem. Phys.*, 2020, 252, p 123242.
40. Y.Q. Lin, and X.M. Chen, *Mater. Chem. Phys.*, 2009, 117, p 125.
41. C. Ang, Z. Yu, and L.E. Cross, *Phys. Rev. B*, 2009, 117, p 125.
42. M. Shi, X.F. Zhang, R.Z. Zuo, Y.D. Xu, L. Wang, L.X. Xie, and G.N. Qiu, *Ceram. Int.*, 2018, 44, p 16624.
43. B. Raneesh, H. Soumya, J. Philip, S. Thomas, and K. Nandakumar, *J. Alloys Compd.*, 2014, 611, p 381.
44. N.S. Negi, R. Kumar, H. Sharma, J. Shah, and R.K. Kotala, *J. Magn. Magn. Mater.*, 2018, 456, p 292.
45. N.M. Parikh, and J.M. Humenik, *J. Am. Ceram. Soc.*, 1957, 40, p 315.
46. Z. Yu, C. Ang, P.M. Vilarinho, P.Q. Mantas, and J.L. Baptista, *J. Appl. Phys.*, 1998, 83, p 4874.
47. A.S. Hassanien, and A.A. Akl, *Phys. B*, 2015, 473, p 11.
48. S.K. Mandal, S. Singh, R. Debnath, A. Nath, and P. Dey, *J. Alloys Compd.*, 2017, 720, p 50.
49. P.J. Bai, Y.M. Zeng, and J. Han, *J. Mater. Sci. Mater. El.*, 2019, 16, p 15413.

Publisher's Note Springer Nature remains neutral with regard to jurisdictional claims in published maps and institutional affiliations.